3D-printed bio-inspired zero Poisson's ratio graded metamaterials with high energy absorption performance

To cite this article: Ramin Hamzehei *et al* 2022 *Smart Mater. Struct.* **31** 035001

OPEN ACCESS
IOP Publishing
Smart Materials and Structures
Smart Mater. Struct. **31** (2022) 035001 (20pp)
https://doi.org/10.1088/1361-665X/ac47d6

3D-printed bio-inspired zero Poisson's ratio graded metamaterials with high energy absorption performance

Ramin Hamzehei[1,2], Ali Zolfagharian[3], Soheil Dariushi[4] and Mahdi Bodaghi[1,*]

[1] Department of Engineering, School of Science and Technology, Nottingham Trent University, Nottingham NG11 8NS, United Kingdom
[2] Department of Mechanical Engineering, University of Manitoba, Winnipeg, Manitoba R3T 5V6, Canada
[3] School of Engineering, Deakin University, Geelong 3216, Australia
[4] Department of Composites, Faculty of Processing, Iran Polymer and Petrochemical Institute, Tehran, Iran

E-mail: mahdi.bodaghi@ntu.ac.uk

Received 11 October 2021, revised 16 December 2021
Accepted for publication 3 January 2022
Published 21 January 2022

Abstract

This study aims at introducing a number of two-dimensional (2D) re-entrant based zero Poisson's ratio (ZPR) graded metamaterials for energy absorption applications. The metamaterials' designs are inspired by the 2D image of a DNA molecule. This inspiration indicates how a re-entrant unit cell must be patterned along with the two orthogonal directions to obtain a ZPR behavior. Also, how much metamaterials' energy absorption capacity can be enhanced by taking slots and horizontal beams into account with the inspiration of the DNA molecule's base pairs. The ZPR metamaterials comprise multi-stiffness unit cells, so-called soft and stiff re-entrant unit cells. The variability in unit cells' stiffness is caused by the specific design of the unit cells. A finite element analysis (FEA) is employed to simulate the deformation patterns of the ZPRs. Following that, meta-structures are fabricated with 3D printing of TPU as hyperelastic materials to validate the FEA results. A good correlation is observed between FEA and experimental results. The experimental and numerical results show that due to the presence of multi-stiffness re-entrant unit cells, the deformation mechanisms and the unit cells' densifications are adjustable under quasi-static compression. Also, the structure designed based on the DNA molecule's base pairs, so-called structure F‴, exhibits the highest energy absorption capacity. Apart from the diversity in metamaterial unit cells' designs, the effect of multi-thickness cell walls is also evaluated. The results show that the diversity in cell wall thicknesses leads to boosting the energy absorption capacity. In this regard, the energy absorption capacity of structure 'E' enhances by up to 33% than that of its counterpart with constant cell wall thicknesses. Finally, a comparison in terms of energy absorption capacity and stability between the newly designed ZPRs, traditional ZPRs, and auxetic metamaterial is performed, approving the superiority of the newly designed ZPR metamaterials over both traditional ZPRs and auxetic metamaterials.

* Author to whom any correspondence should be addressed.

Keywords: zero Poisson's ratio, graded metamaterials, energy absorption, 3D printing, hyperelastic properties

(Some figures may appear in colour only in the online journal)

1. Introduction

Mechanical metamaterials are artificially designed structures obtaining their extraordinary mechanical properties from the specific geometry and configuration of their cells than the parent material from which they are made [1]. Thanks to technological development, in particular 3D printing technology, there are myriads of architected structures possessing diverse mechanical properties. The mechanical metamaterials are divided into main sub-sets, including positive Poisson's ratio (PPR) structures [2], zero Poisson's ratio (ZPR) structures [3–7], negative Poisson's ratio (NPR) structures called auxetics [8–11], negative stiffness [12, 13], and negative thermal expansion structures [14, 15].

There have been numerous studies that have focused on auxiliary structures up to this point. Though the auxetic structures enhance some mechanical properties, in particular the energy absorption capacity due to resisting under compression [16, 17], the merits of ZPR structures are hard to ignore. From the mechanics point of view, due to not existing a relationship between the stress and strain in two orthogonal directions [18], the ZPR value means that there is neither transverse displacement under longitudinal loading nor double curvature under out-of-plane bending. This leads to the ZPRs possess a single curvature (unclastic) under bending compared to the anticlastic and synclastic curvatures of PPR and NPR structures respectively [19].

As ZPR structures exhibit unclastic curvature under bending, they are suitable choices to be used as cylindrical sandwich panels for morphing applications [4, 6, 18, 20], where the structures must undergo pure cylindrical bending or 1D spanwise morphing. It is worth noting that morphing wing designs are classified into in-plane and out-of-plane morphing [21–23], and spanwise morphing is a kind of in-plane morphing. The ZPR structures are also practical in tissue engineering applications [24], in which ZPR scaffolds have similar effects to what natural tissues provide. In the textile industry, the ZPR weaving patterns have also been developed recently [25].

When it comes to categorizing ZPR structures, they can be considered as structures that exhibit ZPR behavior in either one or two orthogonal directions. Bubert *et al* [3] optimized a morphing skin based on accordion topology with chevron bending ligament exhibiting a ZPR behavior in one direction. Similarly, Chen and Fu *et al* [4] modified a semi-reentrant design to obtain a ZPR behavior in one direction. However, some designs show ZPR behavior along with the two orthogonal directions. Dudek *et al* [5] investigated the impact resistance of composite magnetic metamaterials comprising star-shaped ZPR unit cells. Likewise, Wang *et al* [6] designed a reverse semire-entrant structure based on strain-isolation mechanism. In addition, Naghavi Zadeh *et al* [7] designed a fish-based ZPR metamaterial that exhibits a ZPR behavior in both orthogonal directions.

To date, most studies have concentrated on structures comprising uniform unit cells in terms of dimensions and materials. However, from a structural point of view, a structure can be named "graded" with multi-design unit cells, different cell walls thicknesses or even materials [26–28]. The graded structures possess versatile mechanical properties and also possess superiority in terms of energy absorption and mitigating blast loadings than that of the non-graded ones [29]. Lira *et al* [30] investigated the transverse shear stiffness of the thickness-gradient honeycombs numerically and experimentally. They exhibited controllable design properties such as stiffness per unit of weight. Li *et al* [31] introduced piecewise linear graded honeycombs showing better energy absorption under high-crushing speed. Ajdari *et al* [32] realized that the enhancement in energy absorption capacity of honeycombs is a result of the decrease in relative density of the structure along with the crushing direction. Rahman *et al* [33] designed graded honeycomb structures with a diversity of unit cell sizes and materials. Their study showed that the use of multi-material in the fabrication of the structure and significant changes in the size of the unit cells lead to a dramatic enhancement in energy absorption capacity of honeycomb structures.

On the other hand, there are lots of meta-structures whose designs originate from nature or biological aspects. In this regard, Wang *et al* [34] proposed an active structure applying dielectric elastomer on a NPR structure with the inspiration of a human's bone-muscle system to enhance the Young's modulus of a dielectric elastomer. Yang *et al* [35] designed a novel lightweight bio-inspired double-sine corrugated sandwich structure with the inspiration of the dactyl club to boost the impact capacity. Their designs dramatically enhanced the crashworthiness and impact capacity of the sandwich structures compared to the triangular and sinusoidal corrugated sandwich structures. Ha *et al* [36] also designed a novel beetle forewing sandwich panel by mimicking the microstructure of a woodpecker's beak. Their proposed core design possessed high energy absorption capacity compared to the honeycomb core under dynamic loading. Ghazlan *et al* [37] designed a new bone-inspired structure possessing superior energy absorption performance compared to honeycomb and re-entrant metamaterials. Hu *et al* [38] and Zheng *et al* [39] designed double helical metamaterials for energy absorption applications with the inspiration of the DNA molecule. Their design possessed superior mitigation capability and recoverability under compression.

Due to the significant importance of designing energy absorbers to possess the simultaneous considerable energy absorption capacity and stability under compression, this

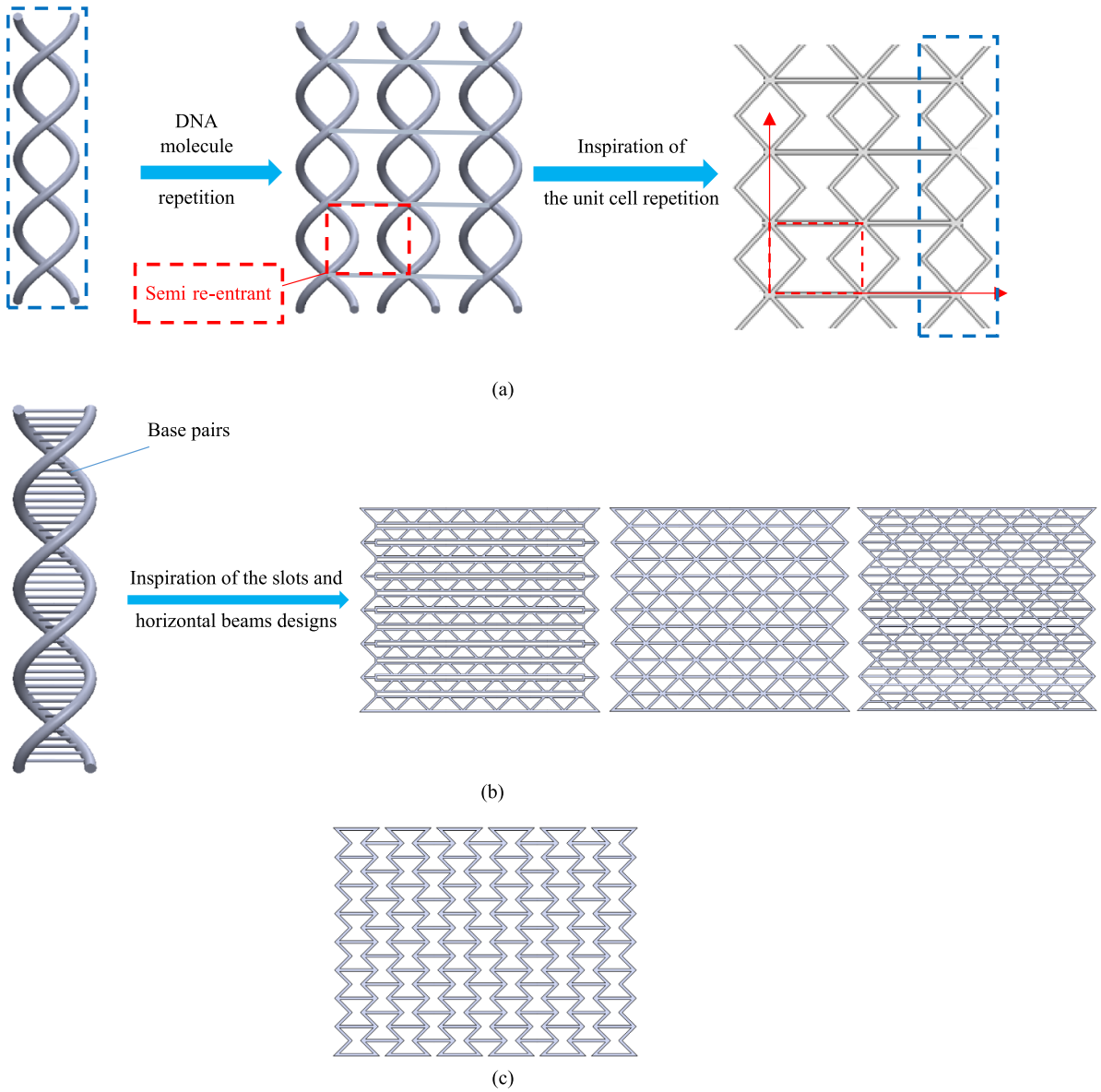

Figure 1. The (a) unit cell repetition pattern, (b) design of slots and horizontal beams inspired by the DNA molecule and (c) conventional auxetic structure.

paper proposes bio-inspired re-entrant based energy absorbers to fulfill those objectives. A 2D image of a DNA molecule demonstrates how a re-entrant unit cell could be patterned along with two orthogonal directions to obtain a ZPR behavior (the provision of stability). Meanwhile, taking slots and horizontal beams into account based on DNA molecule's base pairs leads to considerable enhancements in energy absorption capacity due to a considerable increase in structural stiffness. The ZPR metamaterials comprise multi-stiffness unit cells, so-called soft and stiff re-entrant unit cells. Due to the specific design of re-entrant unit cells, affecting the stiffness of the unit cells, the unit cells' densifications are adjustable under compression. Following that, the mechanical performance and energy absorption capacity of the ZPR metamaterials are evaluated numerically by the finite element analysis (FEA) for each ZPR design. Then, the TPU-based metamaterials are fabricated and tested experimentally to verify the FEA results. Although auxetic structures seem the most suitable choices compared to the rest of the mechanical metamaterials for energy absorption applications, the shrinkage behavior of an auxetic structure itself cannot provide the highest energy absorption capacity. In essence, the structure's stability is another important item that most auxetic structures are incapable of possessing. This is the main reason magnifying the importance of the proposed ZPRs. Furthermore, a comparison between new and traditional ZPRs is carried out, confirming the superiority of the newly designed ZPRs than that of the traditional ZPRs in terms of energy absorption capacity and stability under quasi-static compression.

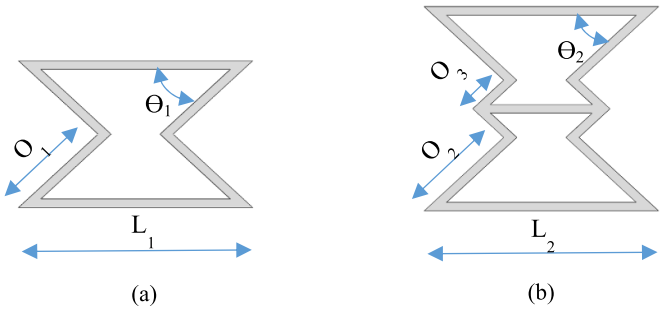

Figure 2. (a) Soft and (b) stiff re-entrant unit cells.

Table 1. Unit cells parameters.

Symbol	L_1	L_2	O_1	O_2	O_3	Θ_1	Θ_2
Value (mm)	12.7	12.7	6.1	6.1	2.4	45 °	45 °

2. Material and methods

2.1. DNA design

The design of ZPR metamaterials is inspired by the 2D image of the DNA molecule's design. The 2D image of a DNA molecule says how a unit cell can be patterned along with the two orthogonal directions to obtain a ZPR behavior. Figure 1(a) shows the way through which a unit cell could be patterned to achieve a ZPR behavior. Meanwhile, figure 1(b) demonstrates how the design of slots and horizontal beams are originated from the DNA molecule's base pairs. These inspirations lead to providing the simultaneous stability and considerable energy absorption capacity for the bio-inspired ZPRs discussing in detail in the next sections. Without inspiring the unit cells' repetition patterns from the DNA, the conventional auxetic structure can be designed (figure 1(c)).

2.2. The geometrical specifications of unit cells

The mechanical performances of the mechanical metamaterials are induced by the specific designs of their unit cells than the chemical compositions of the parent material. This study considers two multi-stiffness re-entrant unit cells, called soft and stiff re-entrant unit cells. The unit cells are shown in figure 2 and the geometrical information is provided in table 1.

2.3. Design of ZPR structures

This study introduces a number ZPR designs based on the multi-stiffness re-entrant unit cells introduced in section 2.2. The designs are named from 'A' to 'N' as depicted in figure 3. To begin, two structures comprising only soft and stiff unit cells are taken into account, so-called structures 'A' and 'B'. Then, the effect of simultaneous existence of soft and stiff unit cells is considered (structure 'C'). Afterwards, the effect of unit cells' arrangements is evaluated (structure 'D'). Next, the consideration of slots and horizontal beams based on DNA molecule's base pairs is investigated (structures 'E' to 'H'). Finally, to boast the capability of the proposed ZPRs compared to conventional ZPRs and even auxetic metamaterials, the structures named 'I' to 'N' are taken into account. The geometrical specifications of the structures are provided in table 2. To have comparable results, the mass of all structures is almost constant around 24 g, otherwise, it has been noted in figure 3. In this way, the wall thickness is a variable parameter through which the mass of all structures is considered constant.

2.4. Material behaviors

When subjected to large deformations, hyperelastic materials are a specific class of materials that respond elastically. They exhibit both a non-linear behavior and large shape changes. This study uses TPU (thermoplastic polyurethane elastomer) as a hyperelastic material to fabricate the structures. To extract the mechanical properties of TPU, five dog-bone samples were 3D printed by fused deposition modelling (FDM) technology according to ASTM D638 Type IV standard tensile test (see figure 4(a)). Mechanical tensile tests were performed by the SANTAM STM-20 universal testing machine with a speed of 5 mm min^{-1} (see figure 4(b)). The stress–strain relationship of TPU is illustrated in figure 4(c). Also, the tensile test specimen undergoes large deformation till the break-down point at the strain of 8.

2.5. Mechanical metamaterials

The TPU-based structures were fabricated by an FDM 3D printer as demonstrated in figure 5. The dimensions of the printed structures are considered constant at 95 × 85 × 10 mm. Compression mechanical tests were conducted using SANTAM STM-20 universal testing machine with a displacement rate of 5 mm min^{-1}. It is also worth mentioning that to avoid the out-of-plane buckling of the structures during compression, the structures were placed into a glassy box. Besides, although the nozzle creates some deficits on the 3D-printed structures mostly caused by high temperature and the flexibility of the material, the deformation patterns can live up to the designers' expectations under compression shown in the next sections.

2.6. Finite element analysis

This study employs ABAQUS/Explicit package to simulate the deformation mechanisms of the ZPR structures under compression.

2.6.1. Boundary conditions. Figure 6 shows the boundary conditions considered in the FEA. The 3D structures are placed between two rigid plates, and then two reference points are assigned to the rigid plates. The bottom reference point is fully constrained along with the three principal directions, while the velocity is applied to the top reference point. Besides, the structure's movement is constrained in the out-of-plane direction to prevent out-of-plane global buckling of

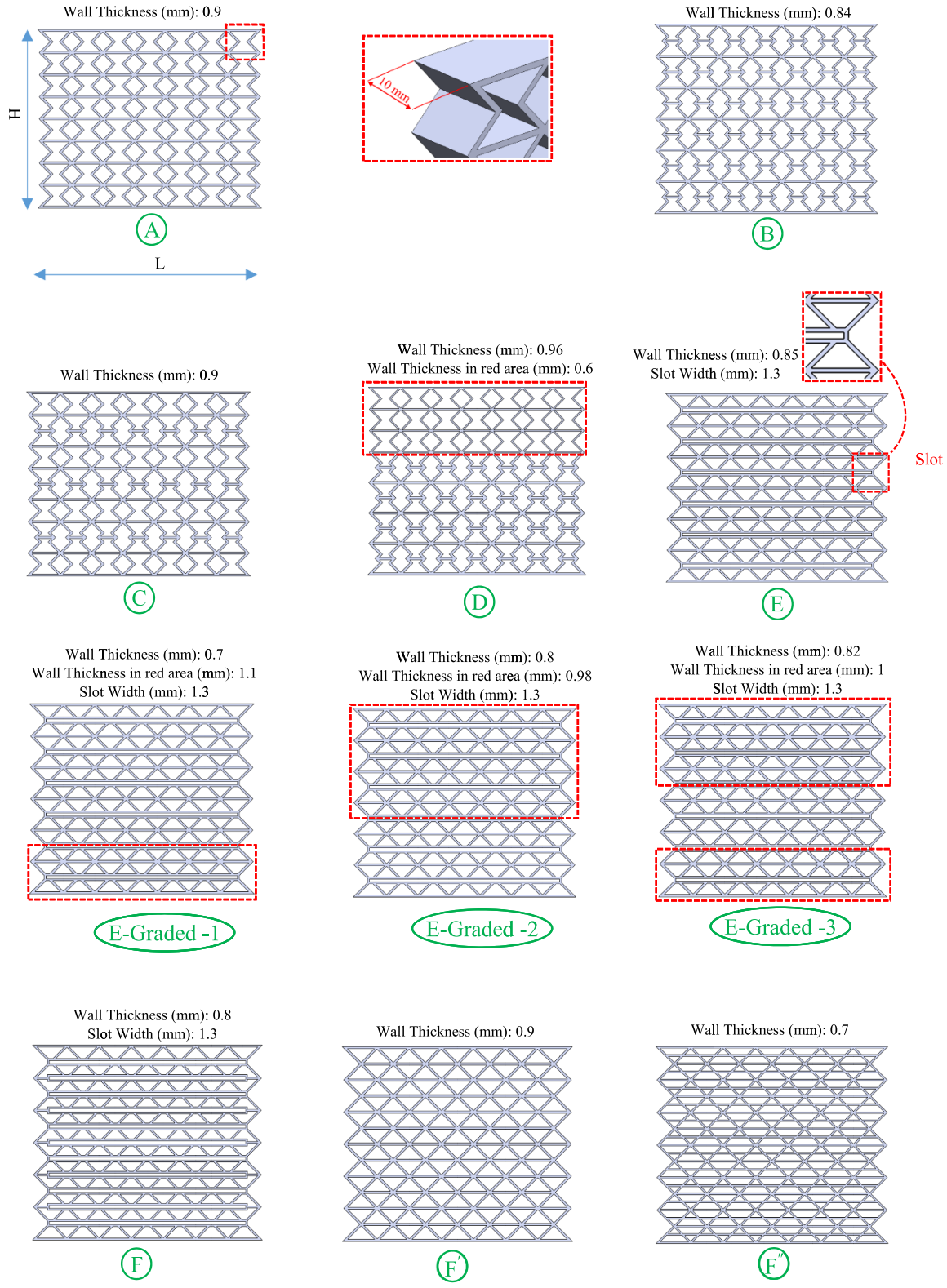

Figure 3. The designed metamaterials.

the structure under compression. To avoid interpenetration, a general contact is defined between the rigid plates and the surfaces.

As dynamic explicit step is used to carry out the FEAs, the velocity must be proper so as to fulfill the quasi-static compression test condition. As the kinetic energy is much less (near zero) than the internal energy by taking the velocity of 1000 mm s^{-1} into account (see figure 7), this speed is considered to simulate the structures' deformation patterns under a quasi-static compression.

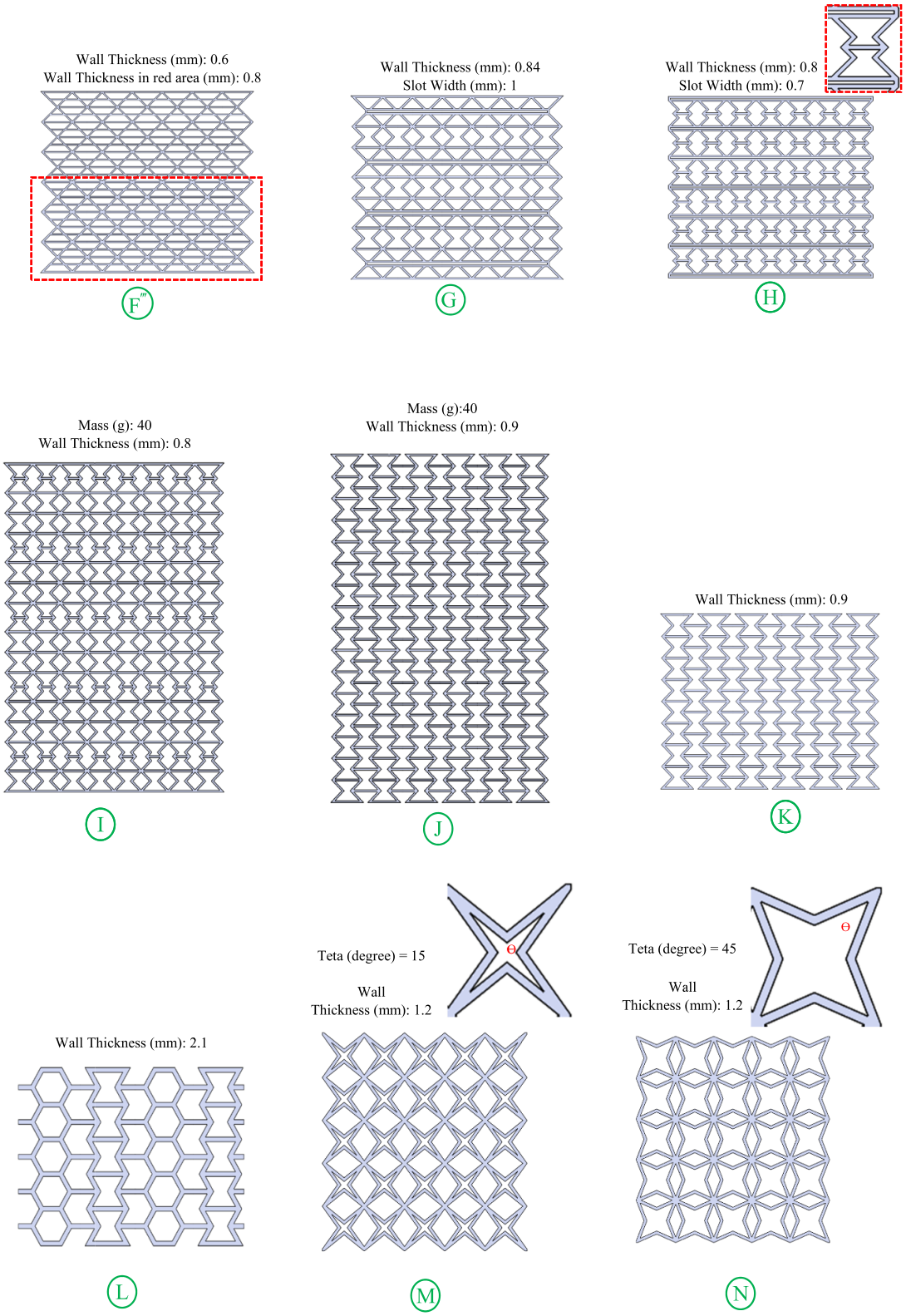

Figure 3. (Continued.)

2.6.2. Hyperelastic model. Hyperelastic materials are considered almost incompressible, indicating that there is no change in their volumes under deformation. The mechanical behavior of the hyperelastic materials is presented by the relations between strain energy density (w) and three strain tensor invariants (I_1, I_2, I_3), or three principal stretches (λ_1, λ_2, λ_3).

$$W = f(I_1, I_2, I_3) = f(\lambda_1, \lambda_2, \lambda_3). \quad (1)$$

Table 2. The geometrical specifications of the structures.

Parameter \ Structure	A	B	C	D	E	E-graded-1
L (mm)	98	98	95	98	95	95
H (mm)	79	83	85	85	85	82

Parameter \ Structure	E-graded-2	E-graded-3	F	F′	F″
L (mm)	95	97	98	98	98
H (mm)	80	82	84	84	84

Parameter \ Structure	F‴	G	H	I	J
L (mm)	98	95	92	113	100
H (mm)	84	85	81	150	130

Parameter \ Structure	K	L	M	N
L (mm)	100	100	85	85
H (mm)	80	80	85	85

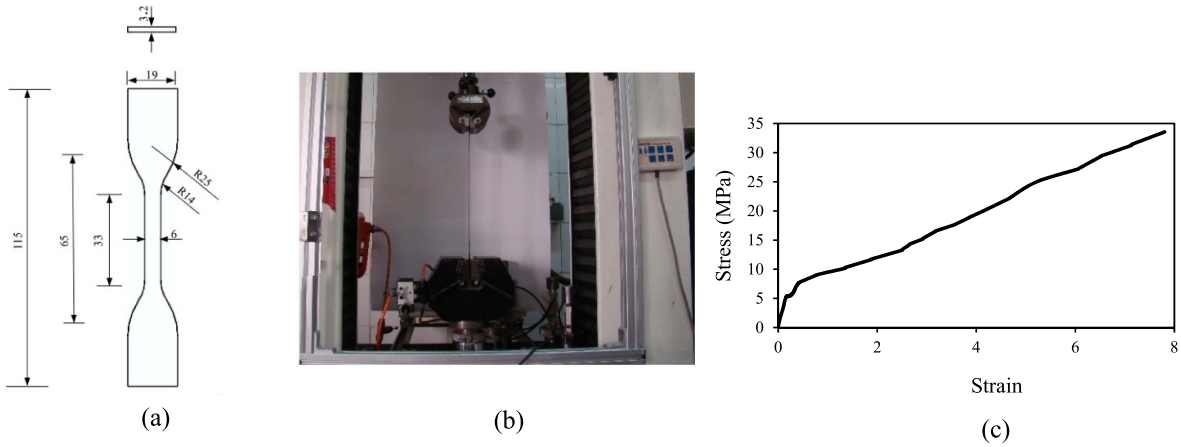

Figure 4. (a) Schematic of standard tensile-testing sample, (b) experimental set up and (c) stress–strain relationship of TPU.

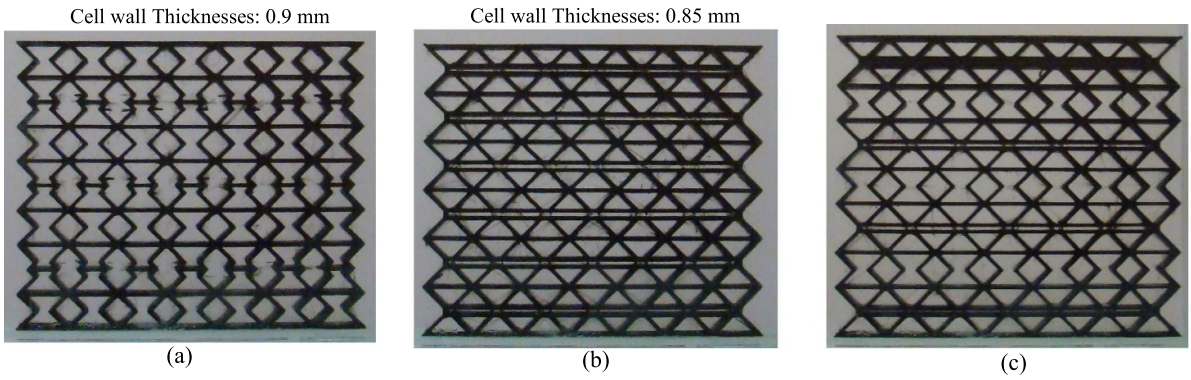

Figure 5. The 3D-printed structure (a) ‘C’, (b) ‘E’ and (c) ‘G’.

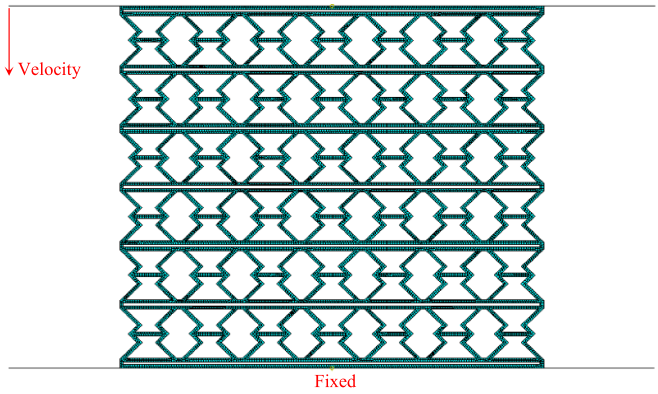

Figure 6. Boundary conditions considered in the FEA.

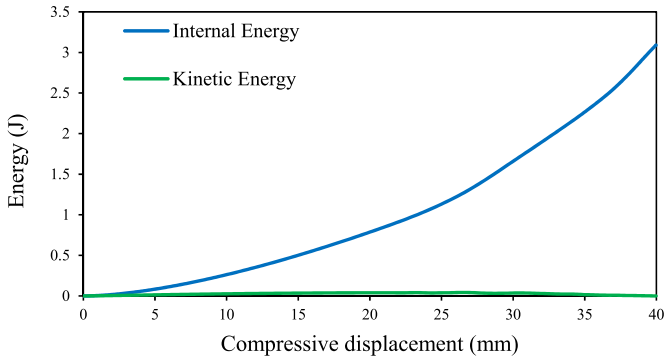

Figure 7. The comparison between internal and kinetic energy obtained from the FEA.

There are diverse types of hyperelastic models, including Neo Hookean, Mooney–Rivlin, Yeoh and Ogden [40]. To perform the FEA on ZPR metamaterials, the Marlow hyperelastic criterion is chosen. It possesses the capability to predict the material response when the results of one mechanical test (uniaxial, equibiaxial or planar test data) are available [41]. To this end, the results of the tensile test (figure 3(c)) are imported to the ABAQUS software.

The Marlow model does not include any explicit relations between the strain energy density and strain invariants. In fact, the strain energy is independent of the second stretch invariant, assumed to be dependent only on the first stretch invariant. The formula related to the Marlow criterion is defined as follows [42]:

$$W = \int_0^{\lambda_T - 1} T(\mathcal{E})\, d\mathcal{E}\,. \tag{2}$$

In equation (2), the parameters $T(\mathcal{E})$ and λ_T are defined as the nominal uniaxial stress and uniaxial stretch respectively.

2.6.3. Element types. As the cell walls possess bending under compression, specifically the bending of soft re-entrant unit cells, 3D solid continuum hexahedral elements with eight nodes, so-called the C3D8R, are taken into account for ZPRs. The R3D4 element type is also considered for each rigid plate.

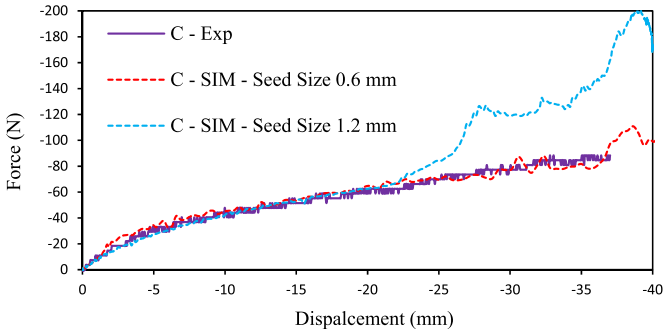

Figure 8. Mesh convergence study.

Also, a convergence study is performed to obtain the most proper element size for achieving accurate results. For that, the seed sizes are changed from 1.2 to 0.6 mm with an interval of 0.6 mm. As the seed size of 0.6 mm possesses an excellent coincidence with the reaction forces obtained from the experiments and FEA (see figure 8), the 0.6 mm of seed size is considered to carry out the FEA.

3. Results and discussions

3.1. Comparison between soft and stiff structures

This section justifies why the unit cells designed in section 2.2 are called soft and stiff unit cells. Also, how much stiffer the stiff unit cell is than that of the soft unit cell. For this purpose, two ZPR structures possessing the same mass are considered, so-called structures 'A' and 'B'. Figure 9 shows the deformation patterns under quasi-static compression from the FEA. As the structure 'A' comprises only the soft re-entrant unit cells, some instabilities occur at high compressive displacements (at 36 mm). On the contrary, the structure 'B' not only resists severely under compression, but it also maintains its stability .

Figure 10(a) compares the force–displacement behaviors of the structures 'A' and 'B' under compression. The curve slop related to the structure 'B' in the elastic region is almost twice greater than the structure 'A', approving the high stiffness of the stiff re-entrant unit cell compared to the soft one. Similarly, the absorbed energy per unit of mass (SEA) in the structure 'B' is nearly twice greater than structure 'A' (see figure 10(b)).

3.2. Deformation patterns

This section discusses the deformation patterns that occur during quasi-static compression test. In general, the ZPR metamaterials are divided into two main groups, those with slots and those without slots. In non-slot ZPR metamaterials, the gradient items are the arrangement of soft and stiff re-entrant unit cells. Figure 11 illustrates the deformation mechanisms in non-slot ZPR metamaterials under compression. As shown in figure 11, the stiff layers lead to the densification of the soft layers, resulting in possessing controllable deformation patterns that allow the designer to arrange the position of the soft and stiff layers according to a specific application. Once the

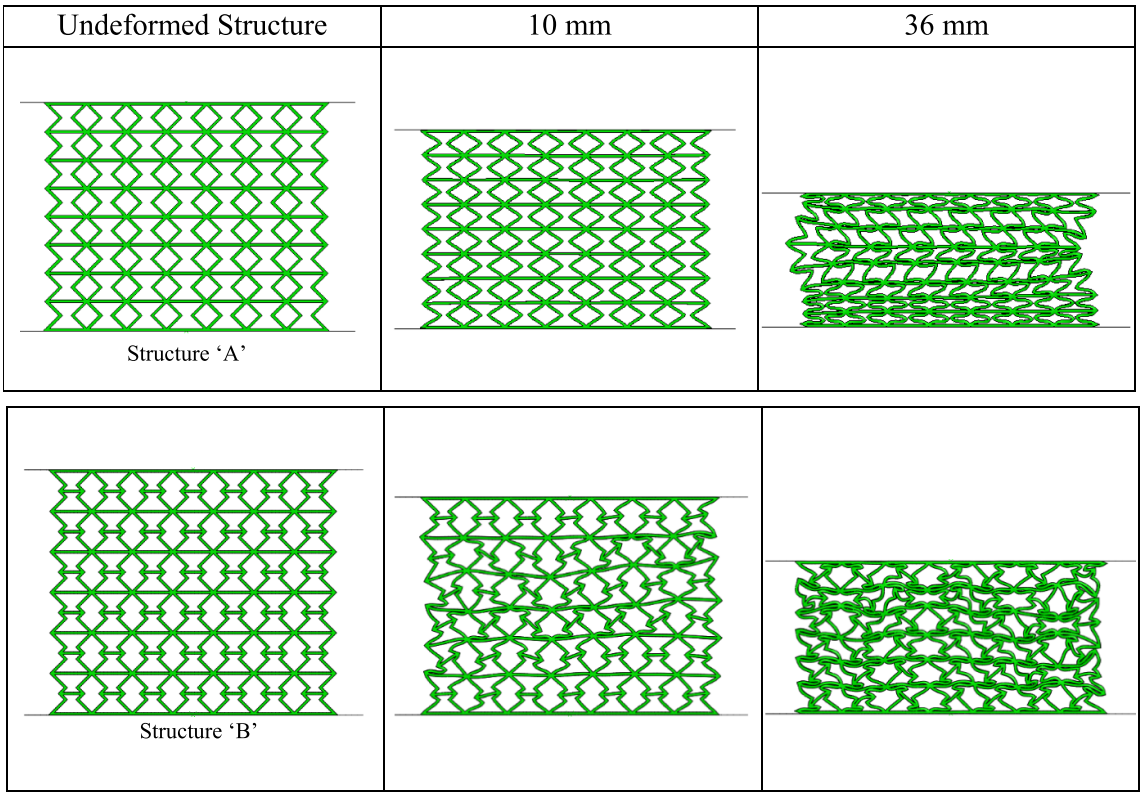

Figure 9. Deformation patterns of the structures 'A' and 'B' under compression.

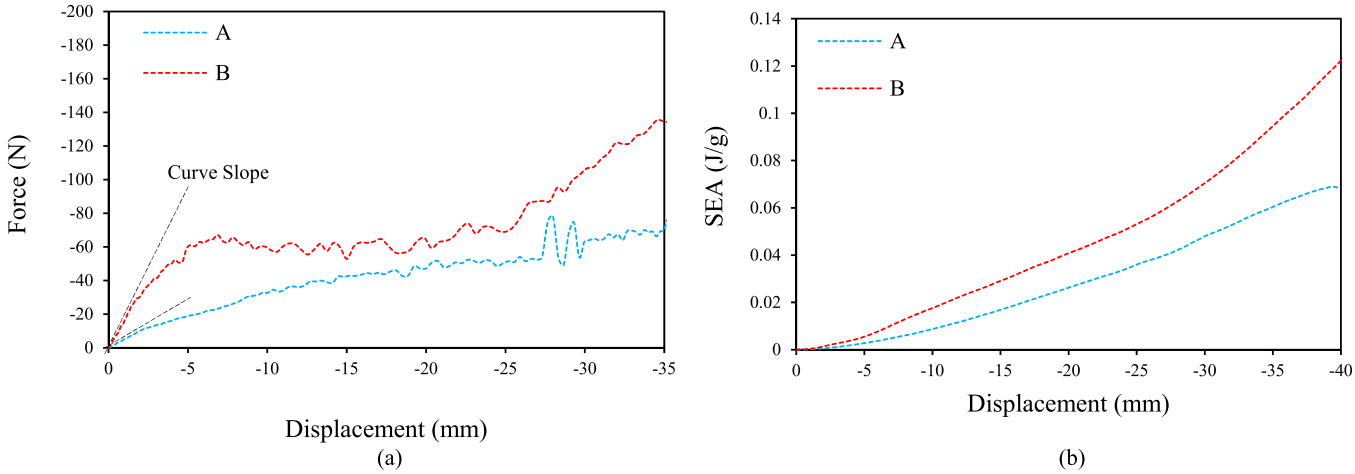

Figure 10. (a) Force–displacement and (b) SEA–displacement relationships of the structures 'A' and 'B' obtained from the FEA.

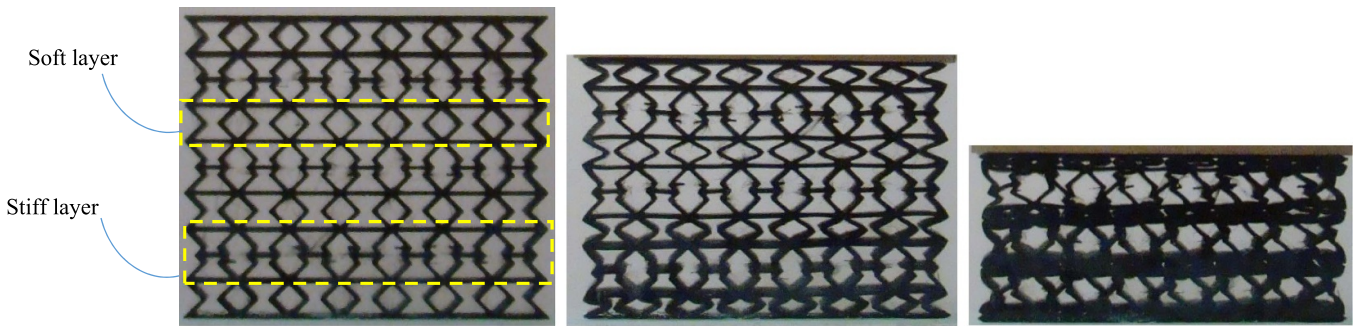

Figure 11. The deformation patterns of the structure 'C'.

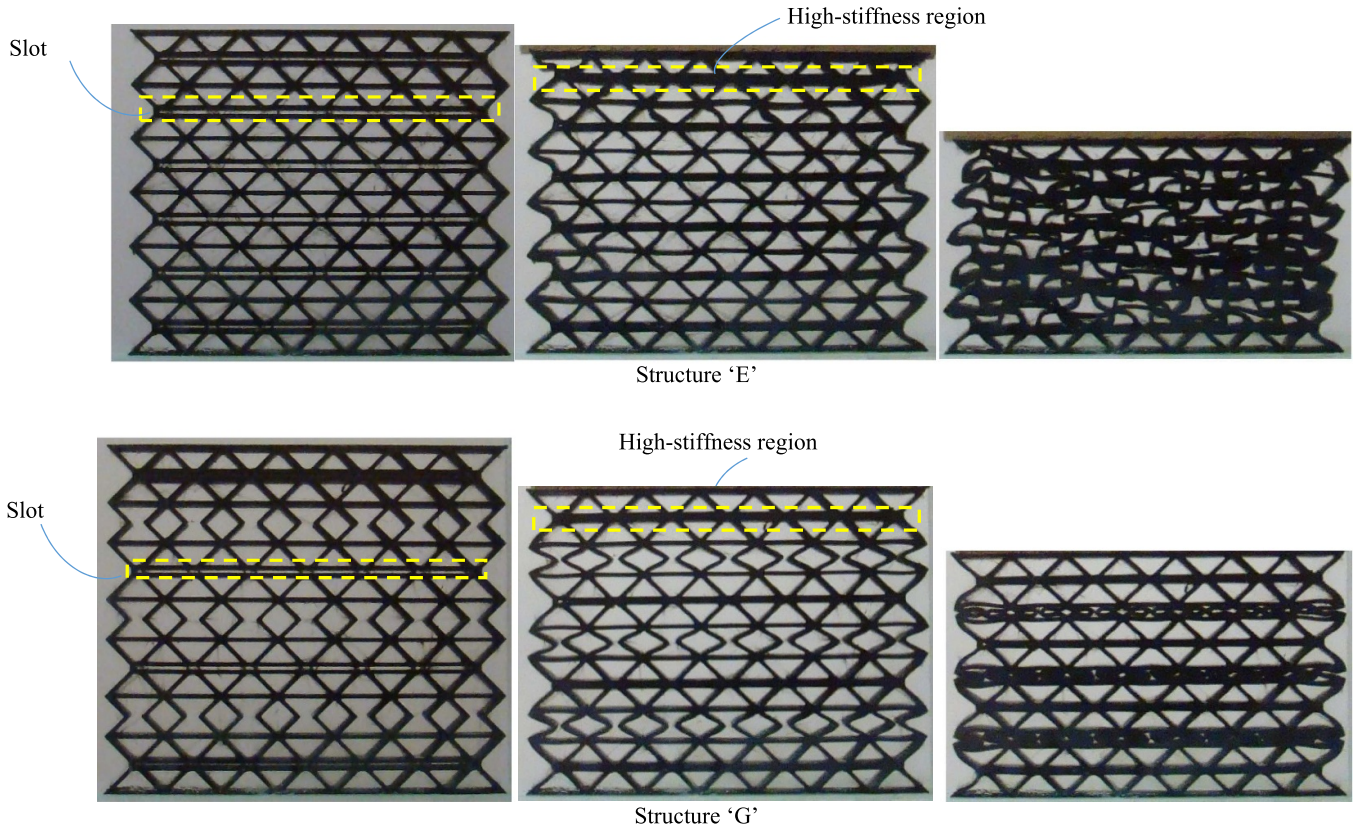

Figure 12. The deformation patterns of the structures 'E' and 'G'.

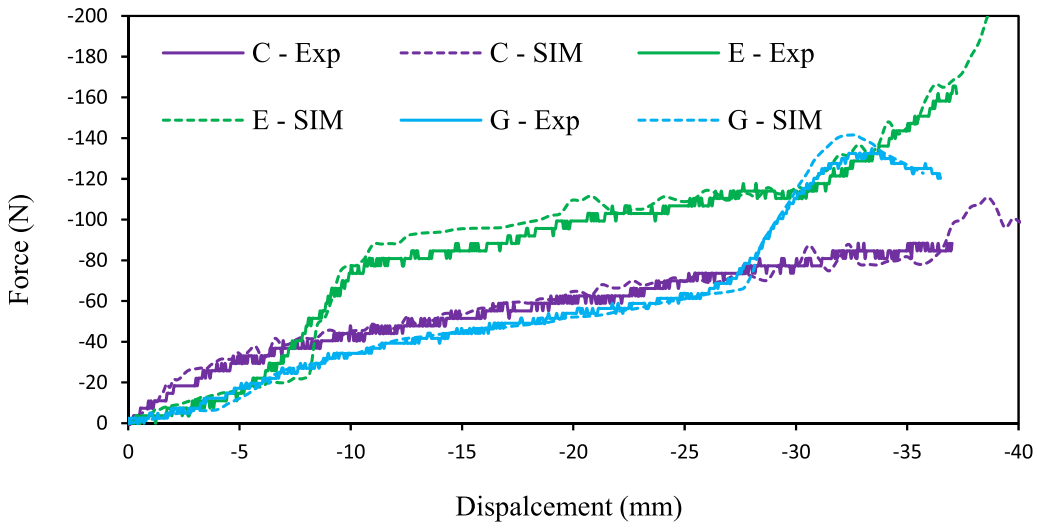

Figure 13. The force–displacement relationship obtained from the FEA and the experiments for the structures 'C', 'E' and 'G'.

compressive displacements are applied, the structure's stiffness increases. The structure's stiffness then decreases due to starting the soft unit cells' densifications. Finally, the structure stiffness increases again due to full densifications of soft unit cells (see figure 13, the purple curve). It is also worth noting that although the soft unit cells experience full densification, the stiff unit cells do not face full densification at high compressive displacements.

The concept of slots in ZPR metamaterials stems from the observation of the base pairs in a DNA molecule (see figure 1(b)). In the ZPR metamaterials comprising slots, by applying compressive displacements, the walls of the slots experience full contact, providing high-stiffness regions in the structure. The high-stiffness regions lead to the occurrence of dominated-bending deformations and buckling in the local unit cells, and the densification occurs at lower

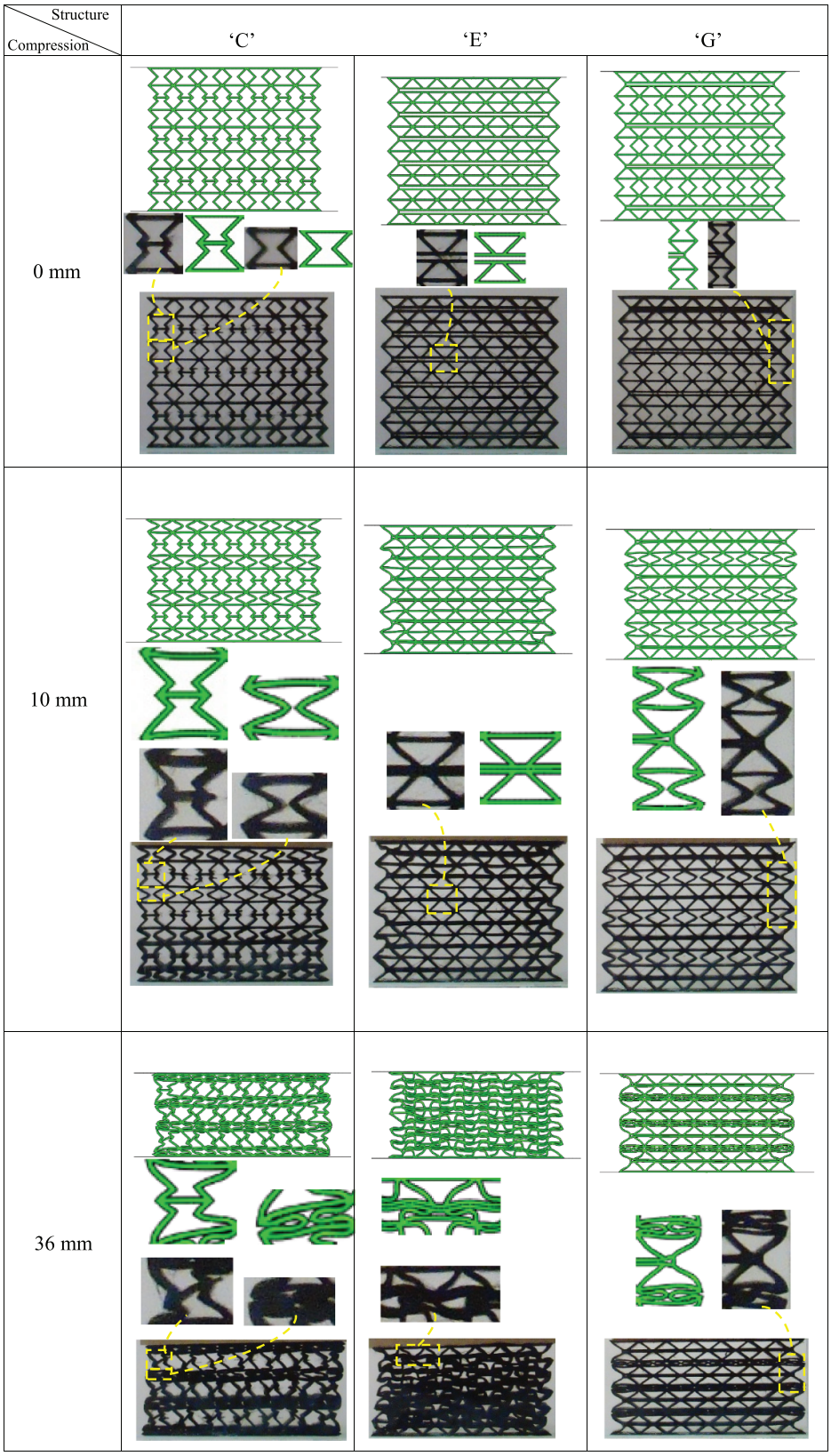

Figure 14. The comparison of deformation patterns between the FEA and experiments.

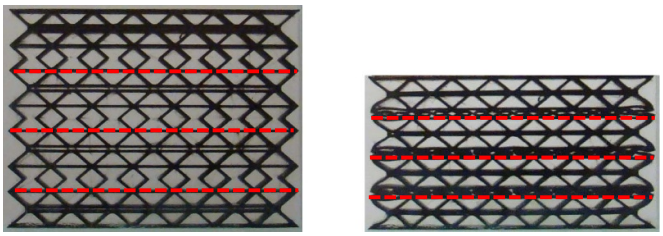

Figure 15. The calculation of Poisson's ratio.

compressive displacements (see figure 12). In essence, the slots lead to an acceleration in the structure's densification by providing an upward trend in force–displacement relationship (see figure 13, green curve). Consequently, not only do the ZPR metamaterials comprising slots possess superior energy absorption capacity, but they also possess stability under compression. Figure 13 shows a close agreement in force–displacement relationship between the experiments and the FEA. Also, figure 14 verifies the deformation patterns between the experiments and FEA.

3.3. The calculation of Poisson's ratio

Poisson's ratio is calculated with a high-resolution digital camera in a fixed position to capture the deformation patterns of the 3D-printed ZPRs. To obtain the Poisson's ratio, the images are extracted and imported to CATIA software. Then, the relative displacements related to each red dashed line are measured (see figure 15). The red dashed lines have the same lengths before and after the compression. By taking the average of the relative displacement of each red dashed line, and dividing it to the axial compressive displacements, the Poisson's ratio is calculated.

3.4. Investigation of energy absorption capacity

Figure 16 shows a group of graded ZPR structures comprising soft and stiff unit cells. When it comes to energy absorption capacity, the ZPR structures designed based on the DNA molecule's base pairs, named E, F, F′ and F″, possess considerable superiority compared to the remaining ZPRs. In structures E and F containing slots, the reaction forces increase slightly under compressive displacements until the full contact of the walls in slots. This leads to providing high-stiffness regions in the structures (shown in the third row of figure 16 by the blue rectangle) and dissipating impact forces via friction. The ZPRs including slots can be practical in the applications where low values of initial reaction forces are required, like collision accidents [43]. However, the structures F' and F" containing more horizontal beams possess a dramatic upward trend in force–displacement relationship upon applying compressive displacements (see figure 17(a)). As can be seen from figure 17, amongst the ZPR structures designed based on the DNA molecule's base pairs, the structure F″ possesses considerable energy absorption capacity compared to the other proposed ZPRs.

3.5. The diversity in cell wall thicknesses

To investigate the effect of different cell walls thicknesses, the structure F‴ and the subsets of the structure E are considered, see figure 18. These structures do not possess constant stiffness and strength due to the variability of the cell wall thickness. The structure F‴ possesses the highest energy absorption capacity amongst all proposed structures in this study, see figure 19. This possession of high energy absorption capacity is caused by the diversity in cell wall thicknesses of structure F‴. This emphasize on the effectiveness of gradient thicknesses as an effective to item to enhance the energy absorption capacity in graded metamaterials.

3.6. Effects of slot widths

This section investigates the influence of slot width in structure 'E' (see figure 20). As can be seen from figure 21, the smaller the slot widths, the stiffer the ZPR metamaterials. In other words, considering small slot width leads to the surge in structural stiffness at lower compressive displacements, and the simultaneous occurrence of bending and cell wall contacts in the local unit cells. This leads to the occurrence of structure's densification at lower compressive displacements, enhancing the energy absorption capacity. Consequently, one possible approach to boost the energy absorption capacity is taking the smaller slot widths into account.

3.7. Effects of wall thickness

To investigate the effects of wall thicknesses, the structure 'E' designed based on the DNA molecule's base pairs is considered. Then, four different cell wall thicknesses with 0. The 25, 0.5, 0.85 and 1.2 mm are taken into account (see figure 22). The thicker walls, the more resistance the walls possess to bend. This leads to an increase in the structure's stiffness, as well as the appearance of plateau region in the force–displacement relation at higher forces (see figure 23(a)), resulting in an increase in energy absorption capacity. As shown in figure 23(b), the amount of SEA increases by up to 1690% when the wall thickness increases from 0.25 to 1.2 mm (the SEA changes from 0.0128505 to 0.23014 (J g^{-1})). Therefore, although the increase in wall thickness leads to an increase in structure's mass, it has a direct influence on energy absorption capacity.

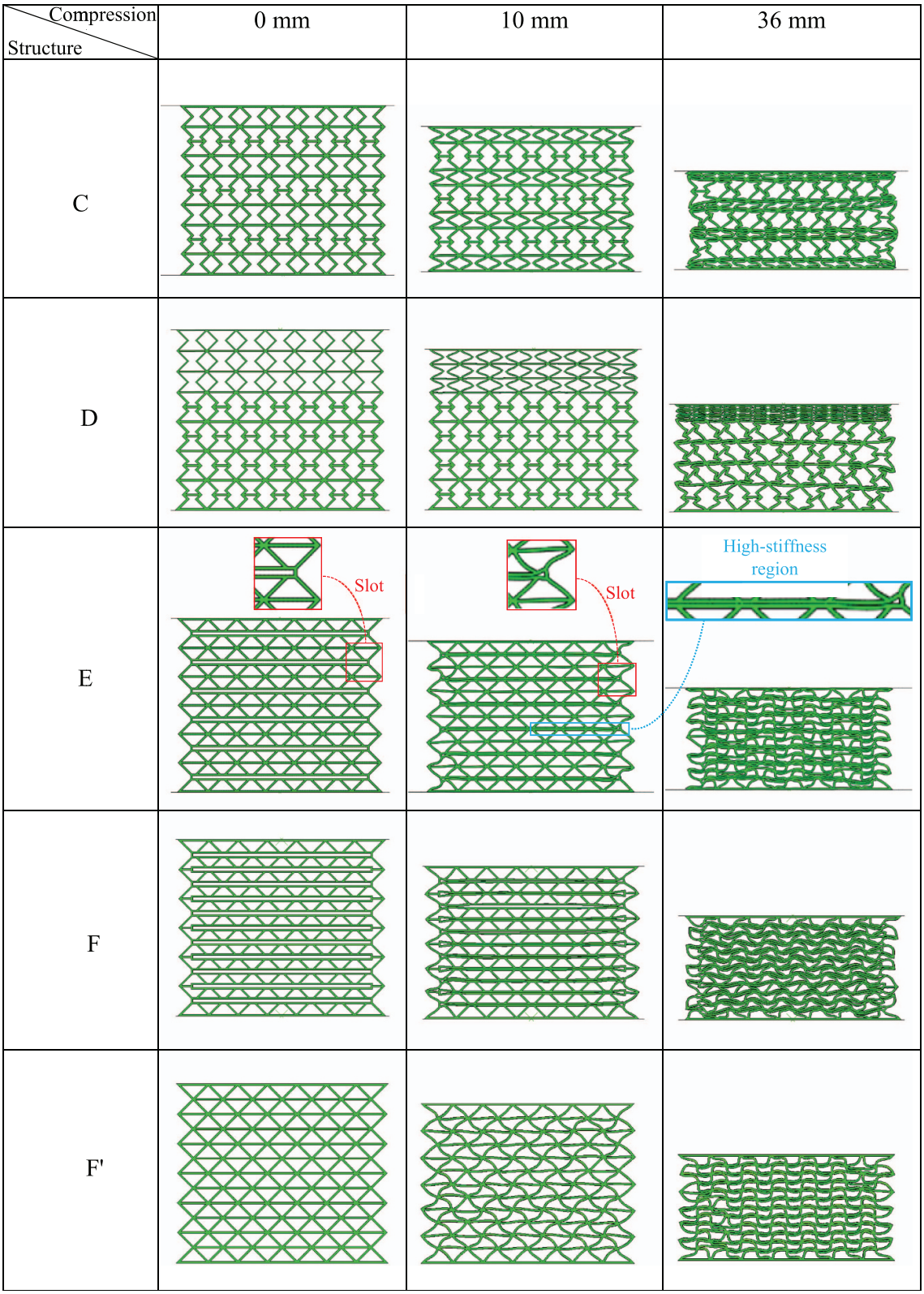

Figure 16. The deformation patterns of the newly designed ZPR structures under compression.

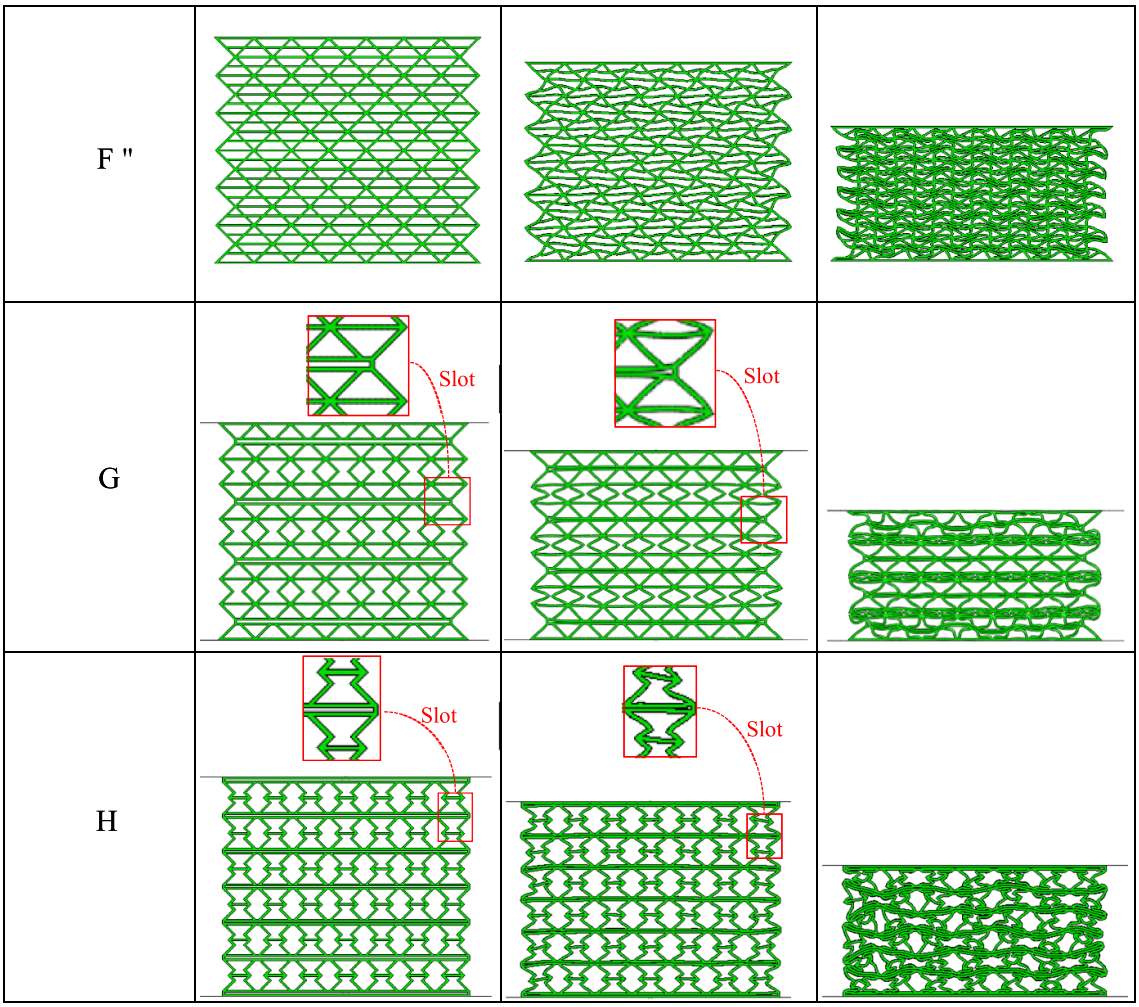

Figure 16. (Continued.)

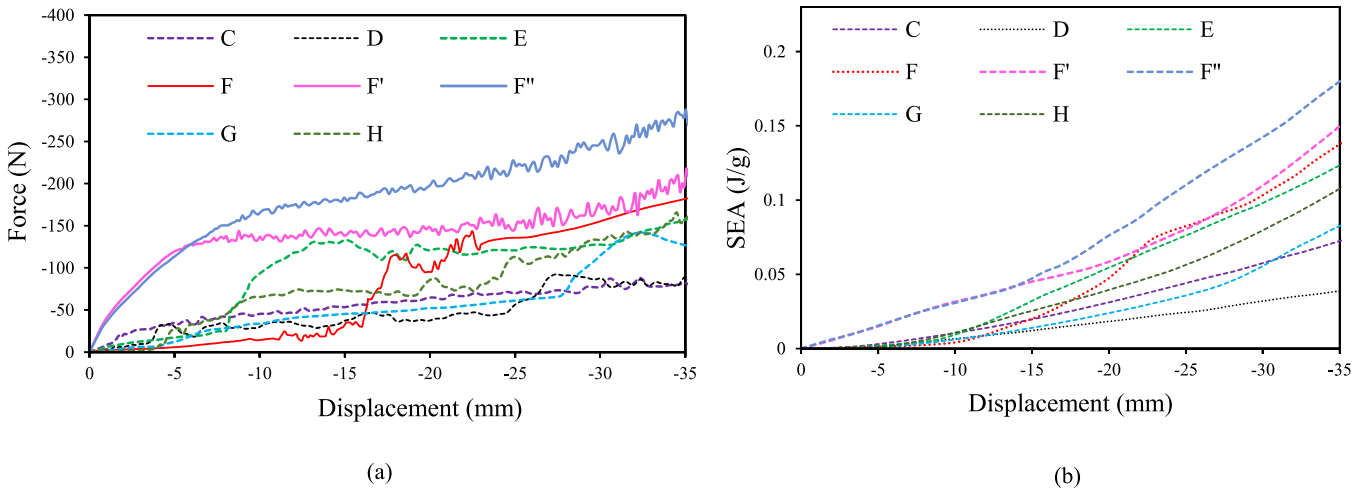

Figure 17. The (a) force–displacement and (b) SEA–displacement relation of ZPR metamaterials obtained from the FEA.

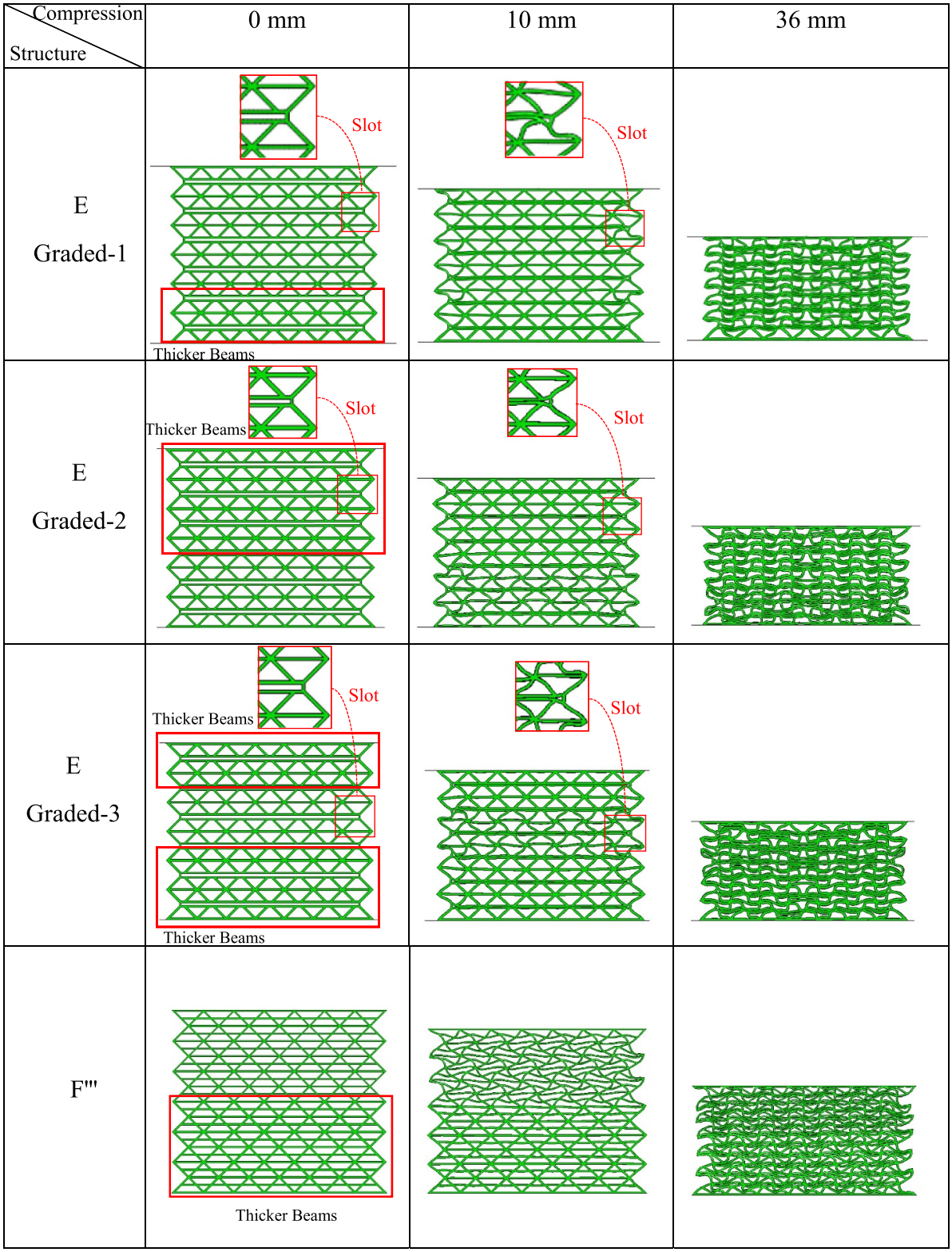

Figure 18. The deformation patterns of the newly designed ZPRs with variable thicknesses under compression.

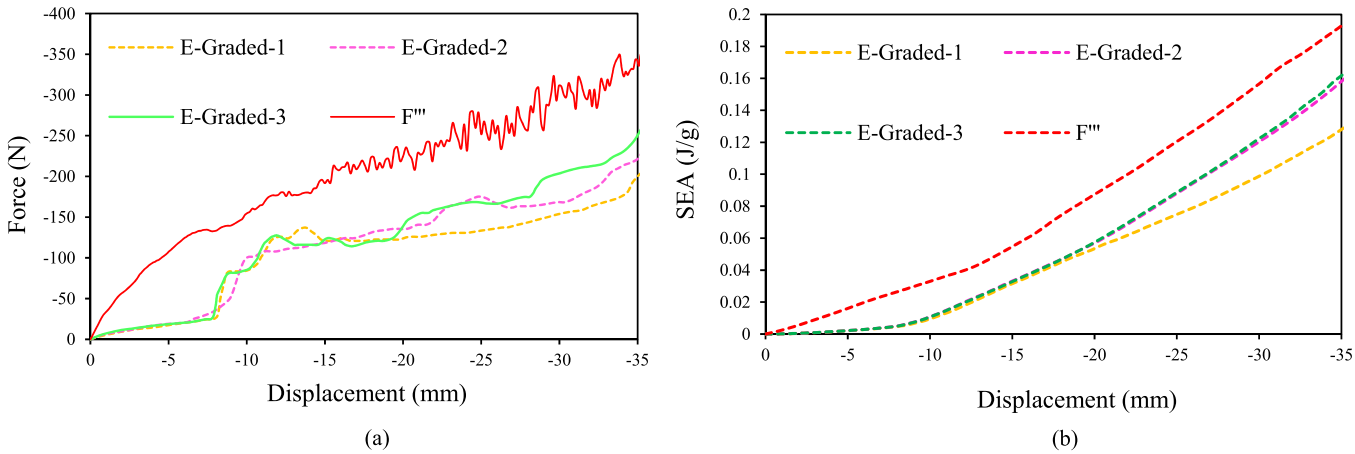

Figure 19. The (a) force–displacement and (b) SEA–displacement curves of the designed ZPRs obtained from the FEA.

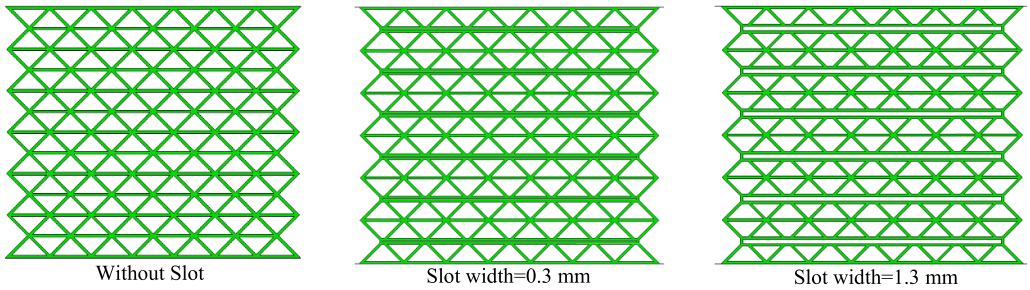

Figure 20. ZPR metamaterials with different slot widths.

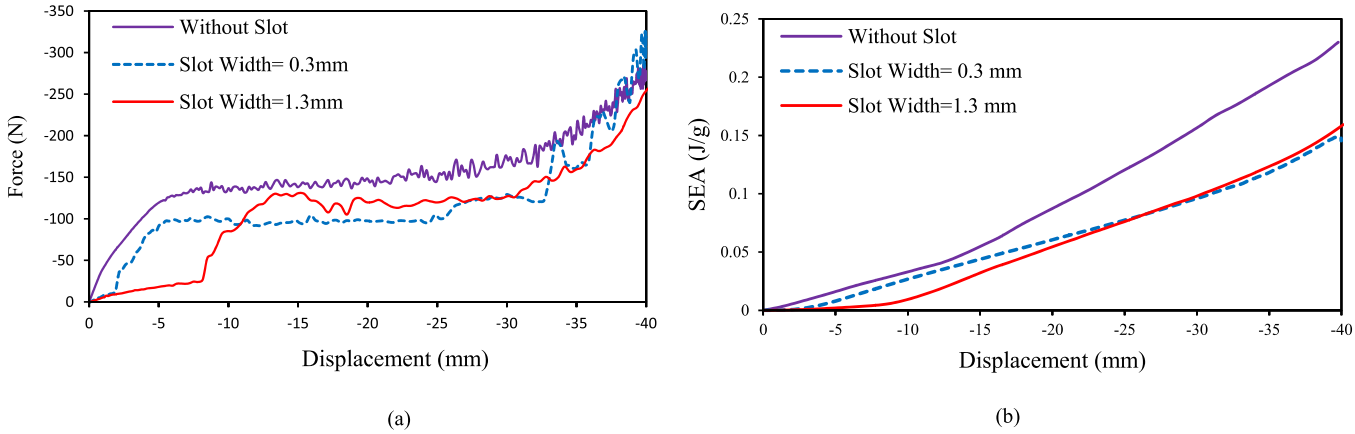

Figure 21. The effect of slot widths on (a) force–displacement and (b) SEA–displacement relationships.

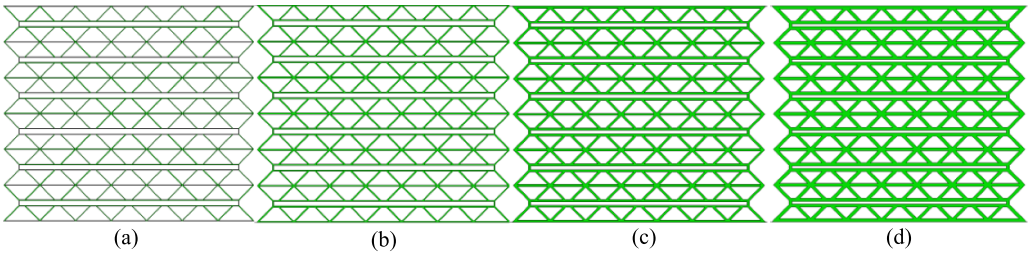

Figure 22. The structure 'E' with (a) 0.25, (b) 0.5, (c) 0.85 and (d) 1.2 mm wall thicknesses.

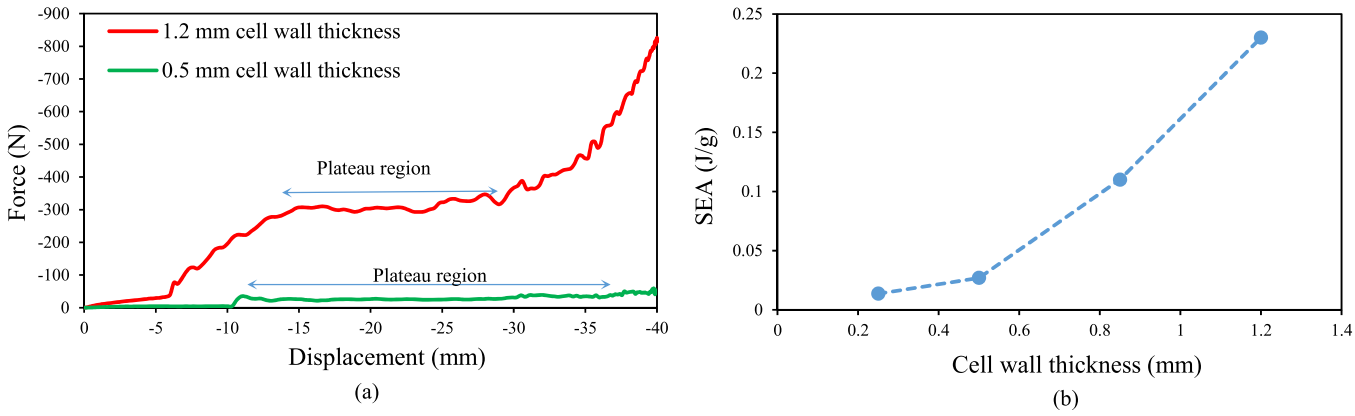

Figure 23. The dependency of (a) force–displacement relationship and (b) SEA on cell wall thicknesses of the structure 'E' obtained from the FEA.

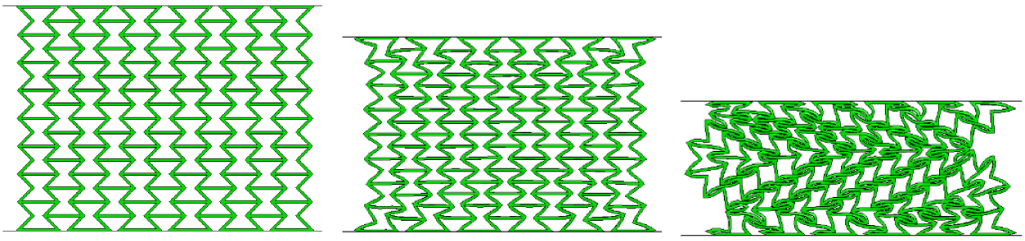

Figure 24. The incapability of an auxetic structure to keep its stability under compression.

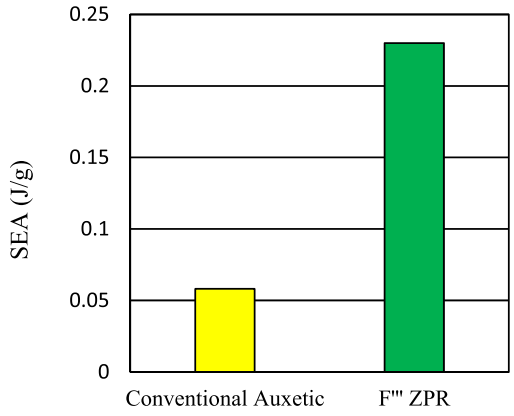

Figure 25. The newly designed ZPR's high energy absorption capacity compared to the auxetic metamaterial.

3.8. Comparison between the bio-inspired ZPRs and auxetic metamaterial

This section exhibits how designing energy absorbers inspired by the DNA molecule's design leads to enhancing the energy absorption capacity compared to the conventional auxetic structure. Also, how the bio-inspired ZPRs' stability is compared with the auxetic metamaterial under quasi-static compression. As can be seen from figure 24, although the conventional auxetic structure shows a shrinkage behavior under compression, it is incapable of possessing uniform shrinkage at high compressive displacements. These are the most common deformation patterns that occur in auxetic structures under quasi-static compression and blast loading [44, 45]. Besides, the energy absorption capacity of the structure F‴ (the ZPR structure possessing the highest energy absorption capacity) is almost four times greater than the conventional auxetic structure's energy absorption capacity (see figure 25).

To demonstrate the superiority of the bio-inspired ZPRs compared to the conventional auxetic structure in terms of stability, two structures with long heights, but with constant mass are taken into account (structures 'I' and 'J'). As can be seen from figure 26, the bio-inspired ZPR metamaterial possesses an excellent stability under quasi-static compression due to layer-by-layer unit cells' densifications.

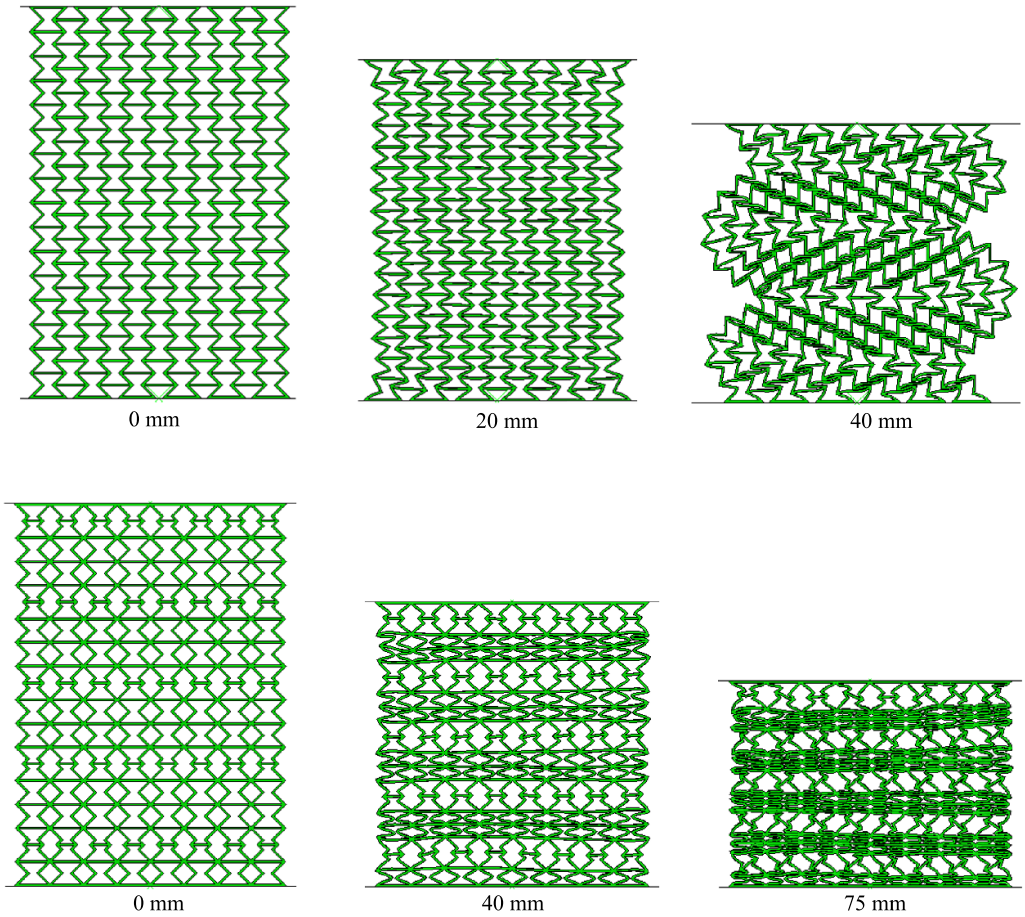

Figure 26. Comparison between the newly designed ZPR and auxetic structure in terms of stability under compression.

Compression / Structure	0 mm	10 mm	36 mm
"L" [20]			
"M" [5]			
"N" [5]			

Figure 27. The deformation patterns of the traditional ZPRs under compression.

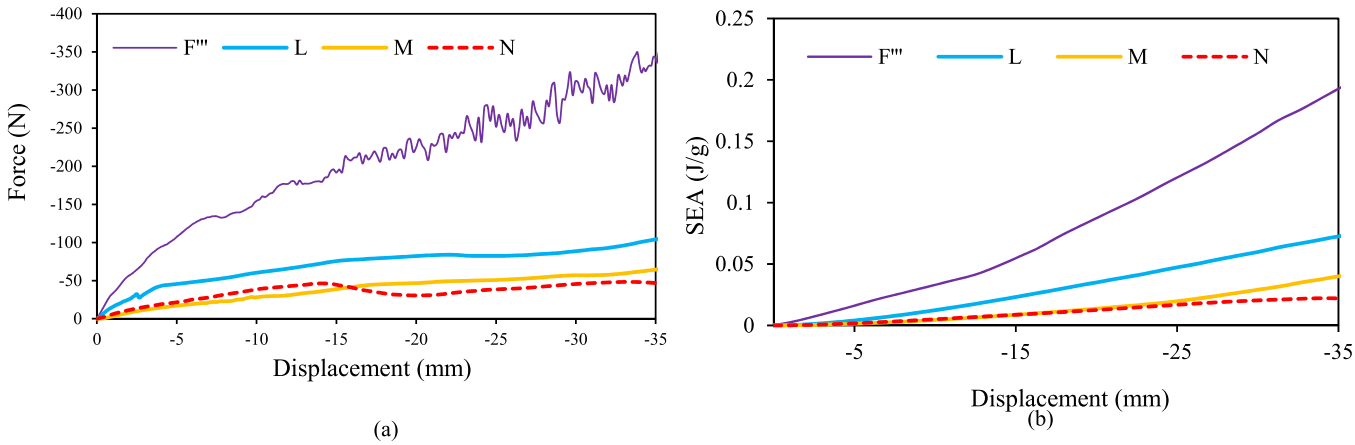

Figure 28. Comparison of (a) force–displacement and (b) SEA–displacement relationships between the newly designed and conventional ZPRs obtained from the FEA.

However, a conventional auxetic structure ong height possesses severe instabilities in the first stages of the quasi-static compression.

3.9. Comparison between the bio-inspired ZPRs with traditional ZPRs

This section considers the structure F‴, possessing the highest energy absorption capacity (see section 3.5), and compares its capabilities in terms of energy absorption capacity and stability with the conventional ZPRs. The traditional ZPRs' deformation patterns are based on the bending and buckling of the cell walls under compression (see figure 27). The stability and high stiffness of structure F‴ is the main differences between bio-inspired and traditional ZPRs. It is also worth noting that the structures 'M' and 'N' possess PPR behavior when the cell walls experience a full contact. In other words, the angle Θ between the two adjacent cell walls (shown in figure 3), provides restrictions for the star-shaped ZPRs to exhibit a continuous ZPR behavior under compression. Figure 28 approves the superiority of the newly bio-inspired designed ZPR over the traditional ones in terms of energy absorption capacity.

4. Concluding remarks

Inspired by the 2D image of a DNA molecule, a new group of 2D ZPR bio-inspired metamaterials was introduced. The ZPRs comprised multi-stiffness unit cells, so-called soft and stiff re-entrant unit cells, to possess high energy absorption performance. TPU-based structures were fabricated by 3D printing and tested mechanically to verify the FEA results. The findings are summarized as follows.

- The DNA molecule's design exhibits the way through which a unit cell can be patterned to achieve a ZPR behavior.
- The DNA molecule's base pairs are the most effective elements providing a considerable enhancement in energy absorption capacity. This increase is caused by providing high-stiffness regions in the newly designed ZPRs under quasi-static compression.
- Due to the variability in the stiffness of soft and stiff re-entrant unit cells, the deformation patterns and unit cells' densifications are controllable under compression.
- Apart from considering slots in ZPR metamaterials, another effective item enhancing the energy absorption performance is the differences in cell wall thicknesses. To have a better understanding, the SEA increases by up to 33% (the SEA changes from 0.158964 to 0.212885) in structure 'E-graded-3′ compared to the structure 'E' with constant cell wall thickness.
- A comparison between the newly designed and auxetic metamaterials is performed. This sheds the light on the incapability of the conventional auxetic metamaterial to keep its stability and the simultaneous possession of high energy absorption capacity under compression.
- Also, a comparison between the newly and traditional ZPRs is performed. This exhibits the superior energy absorption capacity of the newly designed ZPRs compared to the traditional ZPRs.

Data availability statement

All data that support the findings of this study are included within the article (and any supplementary files).

ORCID iDs

Ali Zolfagharian https://orcid.org/0000-0001-5302-360X
Mahdi Bodaghi https://orcid.org/0000-0002-0707-944X

References

[1] Bodaghi M and Liao W H 2019 4D printed tunable mechanical metamaterials with shape memory operations *Smart Mater. Struct.* **28** 045019
[2] Lin K *et al* 2021 Laser powder bed fusion of bio-inspired honeycomb structures: effect of twist angle on compressive behaviors *Thin-Walled Struct.* **159** 107252

[3] Bubert E A *et al* 2010 Design and fabrication of a passive 1D morphing aircraft skin *J. Intell. Mater. Syst. Struct.* **21** 1699–717

[4] Chen Y and Fu M 2018 Mechanical properties of a novel zero Poisson's ratio honeycomb *Adv. Eng. Mater.* **20** 1700452

[5] Dudek K K *et al* 2019 Impact resistance of composite magnetic metamaterials *Sci. Rep.* **9** 1–9

[6] Wang N *et al* 2014 Strain isolation: a simple mechanism for understanding and detecting structures of zero Poisson's ratio *Phys. Status Solidi* b **251** 2239–46

[7] Zadeh N, Mohammad I D and Yasaee M 2020 Fish cells, a new zero Poisson's ratio metamaterial—part I: design and experiment *J. Intell. Mater. Syst. Struct.* **31** 1617–37

[8] Zhou L *et al* 2021 Parametric and experiment studies of 3D auxetic lattices based on hollow shell cuboctahedron *Smart Mater. Struct.* **30** 025042

[9] Günaydın K *et al* 2019 In-plane compression behavior of anti-tetrachiral and re-entrant lattices *Smart Mater. Struct.* **28** 115028

[10] Rezaei S *et al* 2021 Design and modeling of the 2D auxetic metamaterials with hyperelastic properties using topology optimization approach *Photonics Nanostruct.—Fundam. Appl.* **43** 100868

[11] Hamzehei R *et al* 2018 Octagonal auxetic metamaterials with hyperelastic properties for large compressive deformation *Int. J. Mech. Sci.* **145** 96–105

[12] Zhakatayev A, Kappassov Z and Varol H A 2020 Analytical modeling and design of negative stiffness honeycombs *Smart Mater. Struct.* **29** 045024

[13] Tan X *et al* 2019 Novel multidirectional negative stiffness mechanical metamaterials *Smart Mater. Struct.* **29** 015037

[14] Zheng B-B *et al* 2018 A novel re-entrant honeycomb of negative thermal expansion *Smart Mater. Struct.* **27** 085005

[15] Raminhos J S, Borges J P and Velhinho A 2019 Development of polymeric anepectic meshes: auxetic metamaterials with negative thermal expansio *Smart Mater. Struct.* **28** 045010

[16] Chen J *et al* 2020 Mechanical behaviors of 3D re-entrant honeycomb polyamide structure under compression *Mater. Today Commun.* **24** 101062

[17] Hamzehei R *et al* 2020 2D triangular anti-trichiral structures and auxetic stents with symmetric shrinkage behavior and high energy absorption *Mech. Mater.* **142** 103291

[18] Grima J N *et al* 2010 Hexagonal honeycombs with zero Poisson's ratios and enhanced stiffness *Adv. Eng. Mater.* **12** 855–62

[19] Sanami M *et al* 2014 Auxetic materials for sports applications *Proc. Eng.* **72** 453–8

[20] Olympio K R and Gandhi F 2010 Flexible skins for morphing aircraft using cellular honeycomb cores *J. Intell. Mater. Syst. Struct.* **21** 1719–35

[21] Barbarino S *et al* 2011 A review of morphing aircraft *J. Intell. Mater. Syst. Struct.* **22** 823–77

[22] Gomez J C and Garcia E 2011 Morphing unmanned aerial vehicles *Smart Mater. Struct.* **20** 103001

[23] Min Z, Kien V K and Richard L J Y 2010 Aircraft morphing wing concepts with radical geometry change *IES J.* A **3** 188–95

[24] Soman P *et al* 2012 A three-dimensional polymer scaffolding material exhibiting a zero Poisson's ratio *Soft Matter* **8** 4946–51

[25] Zulifqar A, Hua T and Hong H 2018 Development of uni-stretch woven fabrics with zero and negative Poisson's ratio *Text. Res. J.* **88** 2076–92

[26] Wu Y *et al* 2021 Energy absorption of additively manufactured functionally bi-graded thickness honeycombs subjected to axial loads *Thin-Walled Struct.* **164** 107810

[27] Xu F, Zhang X and Zhang H 2018 A review on functionally graded structures and materials for energy absorption *Eng. Struct.* **171** 309–25

[28] Alshaqaq M and Erturk A 2020 Graded multifunctional piezoelectric metastructures for wideband vibration attenuation and energy harvesting *Smart Mater. Struct.* **30** 015029

[29] Novak N *et al* 2019 Crushing behavior of graded auxetic structures built from inverted tetrapods under impact *Phys. Status Solidi* b **256** 1800040

[30] Lira C and Scarpa F 2010 Transverse shear stiffness of thickness gradient honeycombs *Compos. Sci. Technol.* **70** 930–6

[31] Li Z *et al* 2019 In-plane crushing behaviors of piecewise linear graded honeycombs *Compos. Struct.* **207** 425–37

[32] Ajdari A, Nayeb-Hashemi H and Vaziri A 2011 Dynamic crushing and energy absorption of regular, irregular and functionally graded cellular structures *Int. J. Solids Struct.* **48** 506–16

[33] Rahman H *et al* 2021 Energy absorption and mechanical performance of functionally graded soft–hard lattice structures *Materials* **14** 1366

[34] Wang Y *et al* 2018 A bio-inspired novel active elastic component based on negative Poisson's ratio structure and dielectric elastomer *Smart Mater. Struct.* **28** 015011

[35] Yang X *et al* 2017 Crashworthiness investigation of the bio-inspired bi-directionally corrugated core sandwich panel under quasi-static crushing load *Mater. Des.* **135** 275–90

[36] Ha N S, Lu G L and Xiang X 2019 Energy absorption of a bio-inspired honeycomb sandwich panel *J. Mater. Sci.* **54** 6286–300

[37] Ghazlan A *et al* 2020 Performance of a 3D printed cellular structure inspired by bone *Thin-Walled Struct.* **151** 106713

[38] Hu J *et al* 2019 Low-speed impact mitigation of recoverable DNA-inspired double helical metamaterials *Int. J. Mech. Sci.* **161** 105050

[39] Zheng B *et al* 2019 Novel mechanical behaviors of DNA-inspired helical structures with chirality *Int. J. Mech. Sci.* **161** 105025

[40] Tobajas R, Ibartz E and Gracia L 2016 A comparative study of hyperelastic constitutive models to characterize the behavior of a polymer used in automotive engines *Proc. 2nd Int. Electronic Conf. on Materials (May)* pp 2–16

[41] Abaqus ABAQUS user's manual. Version 6.14

[42] Marlow R S 2003 A general first-invariant hyperelastic constitutive model *Constitutive Models for Rubber* vol 15 pp 157–60

[43] Ping X *et al* 2016 Cut-out grooves optimization to improve crashworthiness of a gradual energy-absorbing structure for subway vehicles *Mater. Des.* **103** 132–43

[44] Imbalzano G *et al* 2018 Blast resistance of auxetic and honeycomb sandwich panels: comparisons and parametric designs *Compos. Struct.* **183** 242–61

[45] Dong Z *et al* 2019 Experimental and numerical studies on the compressive mechanical properties of the metallic auxetic reentrant honeycomb *Mater. Des.* **182** 108036